

This is an Open Access document downloaded from ORCA, Cardiff University's institutional repository:<https://orca.cardiff.ac.uk/id/eprint/104108/>

This is the author's version of a work that was submitted to / accepted for publication.

Citation for final published version:

Roberts-Dalton, H. D. , Cocks, A., Falcon-Perez, J. M., Sayers, E. J. , Webber, J. P. , Watson, P. , Clayton, A. and Jones, A. T. 2017. Fluorescence labelling of extracellular vesicles using a novel thiol-based strategy for quantitative analysis of cellular delivery and intracellular traffic. *Nanoscale* 9 (36) , pp. 13693-13706. 10.1039/C7NR04128D

Publishers page: <http://dx.doi.org/10.1039/C7NR04128D>

Please note:

Changes made as a result of publishing processes such as copy-editing, formatting and page numbers may not be reflected in this version. For the definitive version of this publication, please refer to the published source. You are advised to consult the publisher's version if you wish to cite this paper.

This version is being made available in accordance with publisher policies. See <http://orca.cf.ac.uk/policies.html> for usage policies. Copyright and moral rights for publications made available in ORCA are retained by the copyright holders.



Fluorescence Labelling of Extracellular vesicles Using a Novel Thiol-Based Strategy for Quantitative Analysis of Cellular Delivery and Intracellular Traffic.

Roberts-Dalton H.D.¹, Cocks A.², Falcon-Perez J.M.³, Sayers E.J.¹, Webber J.², Watson P.⁴, Clayton A.^{2,*}, Jones A.T.^{1,*}

Abstract

Extracellular vesicles, including exosomes, are naturally derived nanovesicles generated in and released by numerous cell types. As extracellular entities they have the capacity to interact with neighbouring cells and distant tissues and affect physiological processes as well as being implicated in numerous diseases including tumorigenesis and neurodegeneration. They are also under intense investigation as delivery vectors for biotherapeutics. The ways in which EVs interact with recipient cells to influence cell physiology and deliver a macromolecular payload are at the early stages of exploration. A significant challenge within these studies is the ability to label EVs directly or indirectly with fluorescent probes to allow visualization without compromising functionality. Here, we present a thiol-based fluorescence labelling method allowing comprehensive analysis of the cellular uptake of prostate cancer derived EVs in live cells using confocal microscopy. Labelling of the EVs in this way did not influence their size and had no effect on their ability to induce differentiation of lung fibroblasts to myofibroblasts. For endocytosis analyses, depletion of key endocytic proteins and the use of chemical inhibitors (Dynasore, EIPA, Rottlerin and IPA-3) indicated that fluid-phase endocytosis and/or macropinocytosis was involved in EV internalisation. Over a period of six hours EVs were observed to increasingly co-localise with lysosomes, indicating a possible termination point following internalisation. Overall this method provides new opportunities for analysing the cellular dynamics of EVs as biological entities affecting cell and whole body physiology as well as investigating their potential as drug delivery vectors.

¹ Cardiff School of Pharmacy and Pharmaceutical Sciences, Cardiff University, Cardiff, CF10 3NB

² Division of Cancer & Genetics, Tenovus Institute, Heath park, Cardiff University, Cardiff CF14 4XN

³ CIC bioGUNE, CIBERehdParque Tecnológico, Bldg. 801-A, Derio, 48160. Bizkaia SPAIN

⁴ School of Biosciences, Cardiff University, Cardiff, CF10 3AX

1 Introduction

Exosomes, a subpopulation of extracellular vesicles (EVs), are secreted 30-150 nm sized vesicles manufactured within multivesicular endosomes and trafficked to the extracellular space through Rab-GTPase dependent mechanisms ^{1, 2}. These structures comprise a phospholipid bilayer that is particularly enriched in membrane proteins such as tetraspanins, MHC Class-I proteins, integrins and many others ^{3, 4}. The vesicle lumen also encompasses complex entities derived from the cell of origin, including cytosolic proteins and a subset of cellular RNAs ^{5, 6}. Exosomes naturally serve as a means of shuttling this cargo intercellularly as a mode of communication, which can modulate important physiological and pathological processes such as cancer, cardiovascular diseases, and neurodegeneration, as well as in transfer of pathogenic virulence factors ⁶.

This natural ability to functionally transfer a spectrum of macro-molecular cargo between cells raises opportunities for exploiting exosomes as vectors for drug delivery ^{7, 8}. However, little is known about the ways in which exosomes initially interact with the cell, gain intracellular access and are trafficked through the cell to their final destination. Even less is known about how intravesicular cargo is released and directed towards the intended target within the cytosol or other intracellular compartments. The capacity of exosomes to mediate these effects, possibly through endocytosis, requires further characterisation in order to fully understand their natural roles in disease pathogenesis and also unlock their potential for drug delivery.

Endocytosis involves the envelopment of materials from the exterior region of the cell by the plasma membrane. Several endocytic pathways have now been described, each utilising proteins that regulate single and multiple uptake routes ^{9, 10}. Clathrin-mediated endocytosis is by far the most well-defined mechanism, characterised by the formation of a clathrin coated pit that eventually buds into the cytoplasm to form a clathrin coated vesicle that is uncoated before fusing with an early or sorting endosome ⁹⁻¹¹. Endocytosis mediating from distinct platforms of the plasma membrane termed lipid rafts has also been described, with

these processes demonstrating involvement of Caveolin-1^{9, 12} or Flotillin-1^{9, 13}. Other pathways include fluid-phase endocytosis and macropinocytosis, which are defined as cargo non-specific mechanisms, with the latter process demonstrating a reliance on extensive plasma membrane reorganisation by the actin cytoskeleton. This is often in response to growth factor stimulation¹⁴⁻¹⁶. Distinguishing between macropinocytosis and fluid phase uptake as constitutive processes is very difficult as they may share similar protein mediators. Proteins that have been implicated in the organisation of macropinocytosis include PAK-1 and Cdc42 that function as actin regulators¹⁷⁻¹⁹.

Exosome entry and cargo release has been proposed to occur via endocytosis²⁰ and/or through direct exosome-plasma membrane fusion²¹; reviewed in²². These studies labelled purified exosome preparations with fluorescent probes and then used either microscopy or flow cytometry to monitor cell interaction and uptake. Labelling strategies include the use of lipophilic dyes such as PKH26^{23, 24} and the carbocyanine dyes (DiI, DiO)^{25, 26}, which embed non-covalently within the membrane bilayer of the exosome. Such dyes can however form dye aggregates or micelles in aqueous solutions, of similar proportions to exosomes, potentially giving misleading information in uptake experiments²⁷. Exosome permeable compounds including carboxyfluorescein succinimidyl ester (CFSE) and 5(6) carboxyfluorescein succinimidyl diacetate (CFDA) have also been used for this purpose^{20, 28}. Any structural modifications on exosomes following labelling with these dyes will alter their physical characteristics but may also affect their functional properties. For cell uptake analysis this functional impact is rarely considered. Other labelling methods include the use of stable cell lines that fuse Green Fluorescent protein (GFP), or variants of, on to a protein enriched in exosomes, such as the tetraspanin CD63. This consequently produces a sub-population of exosomes, of uncertain proportion, that are GFP-tagged^{29, 30}. This approach also produces cells overexpressing tetraspanins; proteins that are known to be important in the biogenesis and function of these vesicles³¹, and this is therefore a major modification of the composition of the vesicles being produced. Furthermore, tetraspanins are also present on linear membrane fragments, various forms of cellular debris and larger plasma-membrane derived vesicles, and hence does not entirely alleviate the need for rigorous exosome-purifications.

In this report, we have developed a simple and rapid method for covalent fluorescent labelling of purified EVs. The method takes advantage of thiol (sulph-hydryl) groups on the EV surface and our labelling approach does not alter their documented capacity to induce fibroblast differentiation *in vitro*^{32, 33}; suggesting they retain at least a fraction of their biological effects. We thereafter investigated the potential pathways involved in EV uptake, using the well characterised endocytic HeLa cell model. This was performed with chemical inhibitors of endocytic pathways or siRNA-based depletion of specific endocytosis regulating proteins, and thus pathways³⁴. Our findings show that EV uptake is clathrin-independent, with an endocytic profile indicative of macropinocytosis with eventual delivery to lysosomes.

2 Materials and Methods

2.1 Reagents

Transferrin Alexa488 (Tf488), Alexa488/647 10kDa dextran (Dx488/647), C₅-maleimide-Alexa488/633, Cell Mask Deep Red Plasma Membrane Stain, Dulbecco's Modified Eagle Medium (DMEM), Oligofectamine, Opti-MEM I reduced serum medium were purchased from Invitrogen (Paisley, U.K.). Bovine serum albumin (BSA), Dynasore, 5-(N-Ethyl-N-isopropyl) amiloride (EIPA), 1,1'-Disulfanediyldinaphthalen-2-ol (IPA-3) and Rottlerin were obtained from Sigma-Aldrich (Dorset, U.K.). Complete mini-protease inhibitor cocktail tablets were purchased from Roche Diagnostics (Sussex, U.K.). Single sequence (21-23 residues) siRNAs listed in Table 1 were purchased from Eurofins MWG Operon (Ebesburg, Germany). Sucrose and D₂O for EV isolations were from Sigma-Aldrich and Optiseal™ ultracentrifugation tubes from Beckman Coulter.

Table 1. siRNA sequences used to deplete key endocytic proteins

siRNA Target	Sequence	Reference
AP2μ2	GUGGAUGCCUUUCGGGUCAdTdT	Custom designed
Cav-1	AGACGAGCUGAGCGAGAAGdTdT	³⁴
Cdc42	GACUCCUUUCUUGCUUGUdTdT	Custom designed
Flot-1	UGAGGCCAUGGUGGUCUCCdTdT	Custom designed
PAK1	AUAACGGCCUAGACAUUCAdTdT	³⁴
GFP	GGCUACGUCCAGGAGCGCAdTdT	³⁴

2.2 Cell culture

All culture materials were purchased from Invitrogen (Paisley, U.K.). DU145 prostate cancer cells (ATCC) were maintained in Integra Bioreactors (CellLine 1000AD) as described³⁵ with the outer chamber housing RPMI and 5% foetal calf serum (FCS), with the inner cell-containing chamber holding RPMI with 5% FCS that has previously been made devoid of bovine EVs by overnight ultracentrifugation and filtration. All were cultured in a humidified incubator at 5% CO₂, 37°C. Primary lung fibroblasts (AG02262, Coriell Institute of Medical Research) were cultured as sub-confluent monolayers in DMEM F-12 (1:1 mix) supplemented with 10% EV-depleted FCS. HeLa cervical cancer cells (CCL-2; ATCC, Teddington, UK) were maintained in sensi-cell MEM medium supplemented with 10% FCS, as a sub-confluent monolayer.

2.3 Antibodies

Listed antibodies were from the following manufacturers: AP50 (AP2 μ 2) and flotillin-1 BD Transduction Laboratories (Oxford, U.K.); Caveolin-1, GAPDH, PAK-1 Cell Signalling Technologies (Hertfordshire, U.K.); Anti-TSG101, Alix, Calnexin (Santa Cruz Biotechnology, Dallas, TX, USA); anti MHC Class-I (eBioscience, ThermoFisher Scientific, Paisley, UK). Anti-Cdc42 and horseradish peroxidase (HRP) -anti- δ -tubulin (Sigma-Aldrich, Dorset, U.K.); Secondary HRP conjugated goat anti-mouse/anti-rabbit (Thermo-Scientific Pierce, Loughborough, U.K.).

2.4 Extracellular vesicle isolation, purification and characterisation

Using the methodology outlined in Supplementary Information, the isolation and subsequent analyses satisfy the criterion set by the International Society for Extracellular Vesicles (ISEV), for defining this specimen as exosomes³⁶. However, as discussion continues within the field on isolation and characterisation of exosomes as pure entities we refer here on in to our purified particles as EVs.

2.5 Labelling of extracellular vesicles with Alexa488/633

C₅-maleimide-Alexa488 or C₅-maleimide-Alexa633 (200 µg/ml - 2.5 µl) was added to a 30 µl EV aliquot containing 60 to 100 µg protein, and made up to 50 µl with PBS before incubation, with no agitation, for 60 min in the dark at room temperature (R/T). During incubation exosome spin columns (Invitrogen) were prepared according to manufacturer's instructions and powdered resin was hydrated for 15-30 min at R/T. Spin columns placed in the collection tubes were centrifuged for 2 min (750 x g), in a swing-out rotor. The collection tubes were discarded before the addition of the labelled EV aliquot to the resin. Columns were placed in 1.5 ml eppendorf tubes and centrifuged for 3 min (750 x g) to collect labelled EVs. Non-incorporated, excess dye was retained by the resin, and controls involving dye but no EVs were performed in parallel to confirm dye retention by the column. For microscopy analysis, labelled EVs (referred to as EV488 or EV633) were gently mixed to 1000 µl in phenol red free DMEM, before filtration through a 0.22 µm filter (Millex), aliquoted and stored at -80°C until required.

2.6 Fibroblast differentiation assay

To test the impact of labelling on EV function, we used a well-established fibroblast differentiation assay as described³³. Briefly, 80% confluent primary lung fibroblasts (Coriell Institute for Medical Research) were serum deprived for 72 h prior to stimulation with native or fluorescently labelled DU145 EVs (at 200 µg/ml). This dose provides vesicle-associated TGFβ equivalent to a dose of 1.5 ng/ml of soluble TGFβ³². As a positive control, soluble rhTGFβ (Promocell) was used at 1.5 ng/ml. After 72 h, ice cold acetone: methanol (1:1 ratio) was added as fixative for 5 min. Following solvent evaporation in air, cells were blocked in 1% BSA/PBS for 1 h. Monoclonal antibody against alpha-smooth muscle actin (αSMA) (Santa Cruz Biotechnology, Dallas, TX, USA) followed by secondary goat anti-mouse IgG Fab'-Alexa594 conjugate (ThermoFisher Scientific) was used to visualise onset of αSMA stress-fibres. This is a hallmark of the myofibroblastic phenotype visualised by fluorescence microscopy (Zeiss Observer, Cambridge, UK). Fibroblast secretion of Hepatocyte Growth Factor (HGF) was assessed by DuoSet ELISA (R&D Systems), performed on fibroblast conditioned medium 72 h post-treatment, following manufacturers protocol.

2.7 Cell internalisation of Alexa488 labelled extracellular vesicles in HeLa and primary lung fibroblasts

Cells were seeded in 35 mm MatTek imaging dishes (MatTek Corporation, MA, USA) and cultured for 24 h to reach 80-90% confluency. On the day of the experiment, EVs in imaging medium (phenol-red free DMEM, 20 mM HEPES) containing 0.05% w/v BSA were added to cells at 50-60 µg/ml for 30-360 min before live cell confocal microscopy was performed. Cells were incubated with the nuclear label Hoechst for 5 min before washing with imaging medium followed by imaging. For time-lapse imaging, cells were incubated with Hoechst and Cell Mask Deep Red Plasma Membrane Stain (1:5000) for 5 min before washing with imaging medium and time lapse confocal microscopy.

2.8 Labelling of lysosomes with dextran-Alexa647

Cells were seeded to be 50-60% confluent on the day of dextran incubation. Dextran647 (Dx647, 100 µg/ml) was incubated with cells for 2 h (5% CO₂, 37°C), before washing with PBS and re-addition of complete cell culture media. Cells were then incubated for 18 h (5% CO₂, 37°C) before incubating with 50-60 µg/ml EV488 for colocalisation analysis.

2.9 Incubation of cells with Endocytosis inhibitors

All inhibitors were diluted from DMSO stocks to working solutions in imaging medium containing 0.05% BSA. Cells were seeded in 35 mm MatTek dishes 24 h before the day of the experiment to be 80-90% confluent. They were then washed three times with imaging medium containing 0.05% BSA and subjected to 30 min inhibitor pre-incubation with either Dynasore (80 µM), EIPA (25 µM), IPA-3 (50 µM) or Rottlerin (10 µM). Cells were then incubated with the stated concentration of experimental probe (Dx488/647, Tf488, EV488) for the specified time period in the continued presence of the inhibitor. They were then washed with imaging medium prior to performing live cell confocal microscopy.

2.10 siRNA depletion of proteins regulating endocytosis

Performed as described in Supplementary Information.

2.11 Internalisation of Tf488, Dx488/647 into cells

Cells were seeded in 35 mm MatTek dishes and cultured for 24 h to be 80-90% confluent on the day of the experiment. For transferrin uptake analysis, cells were washed three times and incubated with imaging medium supplemented with 0.05% BSA for 30 min before the addition of Tf488 (5 µg/ml) for 15 min. For dextran uptake, 100 µg/ml of Dx488/647 in imaging medium supplemented with 0.05% BSA was added to cells for 60 min without 30 min pre-incubation. Cells were incubated with Hoechst in imaging medium for 5 min before washing with fresh imaging medium followed by performing live cell confocal microscopy.

2.12 SDS PAGE and Western blotting for siRNA depletion

Performed as detailed in Supplementary Information

2.13 Fluorescence Microscopy

2.13.1 Live-cell imaging confocal microscopy

Fluorescent images were taken using a Leica SP5 Confocal Microscope system and captured using LAS AF software. Cells were imaged at R/T with either a 40x 1.25 NA or a 63x 1.4 NA Oil Objective. Alexa488 was excited by a 488 Argon laser (20% intensity), and Alexa633/647 excited by a 633 Helium-Neon laser (20% intensity). Bi-directional, sequential scanning was applied to ensure spectral separation of fluorophores. The presented movie was acquired using the same microscopy settings but with cells maintained at 37°C.

2.13.2 Calculation of Colocalisation Coefficients

To determine the proportion of EVs (green fluorescence) associated with lysosomes (red fluorescence) the M1 Mander's coefficient was calculated using the JaCop ImageJ plug-in

and thresholded using the automated default algorithm. Six fields of view (approximately 60 cells) per time point were analysed and the mean calculated to provide an average colocalisation value for each repeat. The mean of the average colocalisation value for three separate experiments was plotted.

2.13.3 Mean fluorescence intensity (MFI) quantification

Individual cells from LAS AF files were manually selected as regions of interest (ROIs) using ImageJ software. Mean fluorescence intensity (MFI) of each was calculated, resulting in the quantification of approximately 150-160 cells per experimental sample. The geometric mean of each sample group was calculated to provide an average MFI for repeat experiments; the mean of the geometric mean from three independent experiments was calculated and used for statistical calculations.

2.14 Statistical Analysis

To compare control treated samples against experimental samples, a Student's unpaired t-test was utilised using the geometric mean of each separate experiment. Significance was specified as * $p < 0.05$, ** $p < 0.01$, or *** $p < 0.001$.

3 Results and Discussion

3.1 Characterisation and labelling of purified extracellular vesicles

Cells produce a variety of debris and different types of vesicle, we therefore utilised our established approach for the specific isolation of EVs³⁷. Following the clearance of gross debris from cell-conditioned medium, by centrifugation (2000 x g), the medium were filtered (0.22 μm) to remove the majority of larger microvesicles. The medium was thereafter ultracentrifuged, capturing vesicles floating in an isotonic cushion of sucrose, preventing vesicles of classical densities 1.1-1.2 g/ml from pelleting.

Cryo-electron microscopy was performed on EVs purified by this method, revealing the presence of genuine vesicle structures, with a lipid-bilayer boundary (Fig. 1A). There was some heterogeneity in sizes, and the structures are typical for EVs analysed by Cryo-EM as

reported ³⁸. Nanoparticle tracking analysis (NTA) using the NanoSight™ platform, revealed particulates with a modal hydrodynamic diameter of ~100 nm, and a low proportion of larger particulates (Fig. 1B), comparable to sizes seen by Cryo-EM. We also examined the preparation for the presence of proteins typically enriched in EVs. EV-preparations immobilised on microtitre plates were stained with antibodies specific for CD9, CD81, CD63 and respective isotype-matched controls.

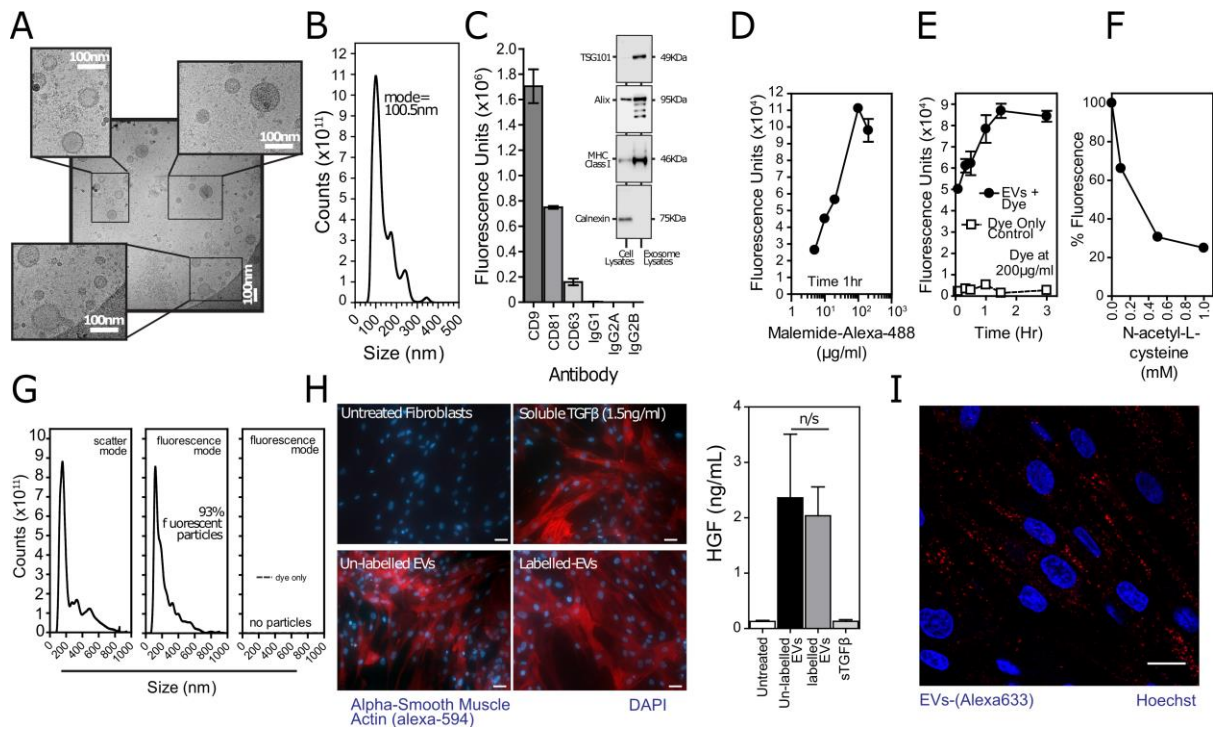


Fig.1. Labelling of EVs with maleimide-Alexa488. (a) Cryo-electron microscopy of a typical preparation of DU145 EVs, with examples of small vesicular structures. Higher magnification micrographs highlight some heterogeneity in sizes. (b) Nanoparticle tracking analysis of DU145 EV size distribution. (c) Plate-immobilised EVs with surface staining for tetraspanin proteins, as indicated. (c, inset) western blot panel with cell lysates compared to EV lysates (each with 20 μg protein / lane), stained for exosomal or cellular markers as indicated. (d) Maleimide-Alexa488 (5 - 200 $\mu\text{g}/\text{ml}$) was incubated with EVs for 1 h prior to separation of free dye and analysis by fluorimetry. (e) EVs were labelled with maleimide-Alexa488 at 200 $\mu\text{g}/\text{ml}$ up to 3 h (circles) and retention of free dye by the column (squares). (f) EVs were pre-incubated with N-Acetyl-Cysteine up to 1 mM for 30 min prior to labelling with maleimide-488 (200 $\mu\text{g}/\text{ml}$ for 1 h). (g) Maleimide-Alexa488 labelled EVs analysed by NTA, (left) shows a similar size distribution profile measured in light scatter mode or measured with fluorescence filter revealing high proportion of fluorescent vesicles (middle); absence of fluorescent dye-particles in the absence of EVs (right). (h) Growth arrested fibroblasts were stimulated with treatments as indicated, and 72 h later fixed and stained for detection of α -smooth muscle actin (red, Scale bar: 50 μm). (h, bars) Medium harvested from stimulated fibroblasts after 72 h, were assessed for levels of HGF by ELISA, showing mean \pm Standard Deviation of triplicates. N/S: Not significantly different, n=3. (i) Primary lung fibroblasts were incubated with maleimide-633 labelled EVs (60 $\mu\text{g}/\text{ml}$) for 1 h before live cell confocal microscopy was performed. Cells were incubated with Hoechst for 5 min before imaging to label the nucleus. Scale bar: 20 μm .

This highlighted strong, specific signals for these tetraspanins (Fig. 1C), which is a particular trait of exosomes³⁹. In addition, by comparing the parent DU145 cancer cells with EV preparations by western blotting, we also reveal an enrichment of some classical EV-associated proteins such as TGS101, Alix and MHC Class-I (Fig. 1C, inset). In contrast, the

endoplasmic reticulum marker, Calnexin, was not detectable in these preparations, yet abundant in cell lysates, demonstrating the paucity of cellular contamination of these EV preparations. Furthermore, using a combination of BCA-protein assay and NanoSight™-concentration measurements, the particle to protein ratio for purified EVs was calculated. This gives an indication of specimen purity as we describe ⁴⁰ and for all preparations used in the study a particle : protein ratio of $>2 \times 10^{10}$ particles/ μg protein was achieved.

The EV is an environment that is cysteine rich, through, for example, the presence of tetraspanin webs ³⁹. We therefore postulated that the thiol (-S-H groups) present on these structures would react with a maleimide functional group, to form a stable, non-reversible, thio-ether linkage. Fluorophore conjugated maleimides are often used to fluorescently label bio-molecules and here we used C₅-maleimide conjugated to Alexafluor488. Other groups have exploited this labelling protocol in order to study micro-particle populations whereby whole blood samples were labelled with BODIPY-maleimide for analysis via flow cytometry ^{41, 42}. However, BODIPY itself is used to label membranes, and is therefore likely to integrate onto the EV bilayer.

We examined the capacity for maleimide-Alexa488 to react with EV thiols. Part of this procedure however, involves the removal of non-bound dye from the EV-preparations. Initial experiments used ultracentrifugation washes to achieve this, but the method was refined thereafter by using a spin-column (Invitrogen), that retains molecules of $<3000\text{Da}$. Initial experiments explored incubating a constant quantity of purified EVs with varying fluorophore concentrations (Fig. 1D), showing saturating levels of labelling at $\geq 100 \mu\text{g/ml}$ after an incubation of 1 h. At the saturating fluorophore concentration $200 \mu\text{g/ml}$, we also examined various incubation times revealing most of the fluorophore-EV labelling occurs very rapidly within the first 5 min, and saturation was reached at 1 to 2 h (Fig. 1E, circles). A control for fluorophore-only (no EVs) to assess its possible retention by the spin column is also shown, revealing negligible signal (Fig. 1E). We chose labelling conditions of $200 \mu\text{g/ml}$ for 1 h for the remainder of the study. To ascertain whether or not the fluorophore was actually forming a covalent bond through the thiol groups, or merely binding passively to the vesicle surface, we added a competitor that works by capping the available reactive thiol groups. Pre-incubating EVs with doses of N-acetyl-L-cysteine showed a potent ($\sim 80\%$) inhibition of labelling under these same conditions (Fig. 1F).

Nanoparticle tracking analysis revealed a similar size distribution profile following incubations with maleimide-Alexa488, suggesting a paucity of gross complexation due to maleimide-vesicle cross-linking (Fig. 1G, left). Importantly, NTA-analysis in the presence of a low-pass 500 nm filter showed the majority (>90%) of vesicles were fluorescent (Figure 1G, middle). The capacity to monitor fluorescent nanovesicles by this method is a challenge, and successful tracking here points to strong fluorescence output from each vesicle. We also analysed the stock maleimide-Alexa488 reagent, by NTA. Unlike for some other fluorescent labels, particularly PKH26, there were negligible particles detected in scatter mode, and there were no particles seen with a fluorescent filter in place (Figure 1G, right graph). An example of nanoparticulate PKH26 fluorescent aggregates in the absence of EVs are shown (Fig. S1). Particulate material spanning the size range of exosomes was present in the stock solution, and a high proportion (52%) of these are fluorescent. We conclude this method is a simple, rapid and highly effective modality for EV labelling, and is free of artefacts related to insoluble dye nanoparticulate.

We next investigated the functional impact of coating EVs with our fluorescent label; an aspect that is rarely considered in previous studies. To do this, we relied on a well-established functional assay whereby prostate cancer exosomes trigger the differentiation of fibroblasts to myofibroblasts³². This process requires delivery of exosome-associated TGF β to fibroblasts, but also is likely to involve additional exosome-cargo as the myofibroblasts generated are distinct from those formed by soluble TGF β -stimulation in that secretion of Hepatocyte growth factor (HGF) is triggered³³. Stimulation of fibroblasts either with native or with maleimide-Alexa488 labelled EVs successfully triggered the onset of stress fibres visualized via α SMA labelling; soluble TGF β also did this as expected (Fig. 1H). When evaluating the secretion of HGF however, there was clear difference in levels of HGF whether stimulations were by EVs or soluble TGF β (Fig. 1H, bars), as we have previously observed³³. The labelled or unlabelled EVs were equally proficient at stimulating HGF secretion.

In this assay, which represents a major and complex cell differentiation process, our maleimide-Alexa488 labelling approach shows no signs of attenuating EV function.

3.2 Endocytic analysis of Alexa488 extracellular vesicles in cells

We investigated the possibility of visualising the labelled EVs following incubation with the fibroblasts. These cells had high background cellular autofluorescence at 488nm excitation (Data not shown) and the purified EVs were therefore labelled with Alexa633 using the same procedure. Fig. 1I demonstrates these EVs were internalised to label punctate structures indicative of endosomes. These cells are however poorly characterised with respects to characterisation of endocytosis. We and others have performed detailed studies of the involvement of individual endocytic pathways in HeLa cells as model for uptake of drug delivery vectors ³⁴. Previous studies on exosome and EV uptake have also been published using HeLa cells ^{30, 43, 44}. We therefore decided to focus our subsequent experiments on the well characterised HeLa cell line.

HeLa cells incubated with Alexa488 labelled EVs (EV488) for 30 and 60 min demonstrated a scattered punctate distribution throughout the cell cytoplasm (Fig. 2A). Time lapse imaging of EV488 incubated with HeLa cells over a period of 3 min (after a 120 min pre-incubation) shows these structures to be highly motile with little evidence of extensive accumulation at the plasma membrane (Video. S1). There was a noticeable time dependant increase in fluorescence intensity from 30 min to 240 min (Fig. 2B) and at this later time point fluorescence was more polarised to the perinuclear regions. This confirmed that these labelled EVs also have endocytic capacity in this cell line, allowing further analysis of cell entry mechanisms.

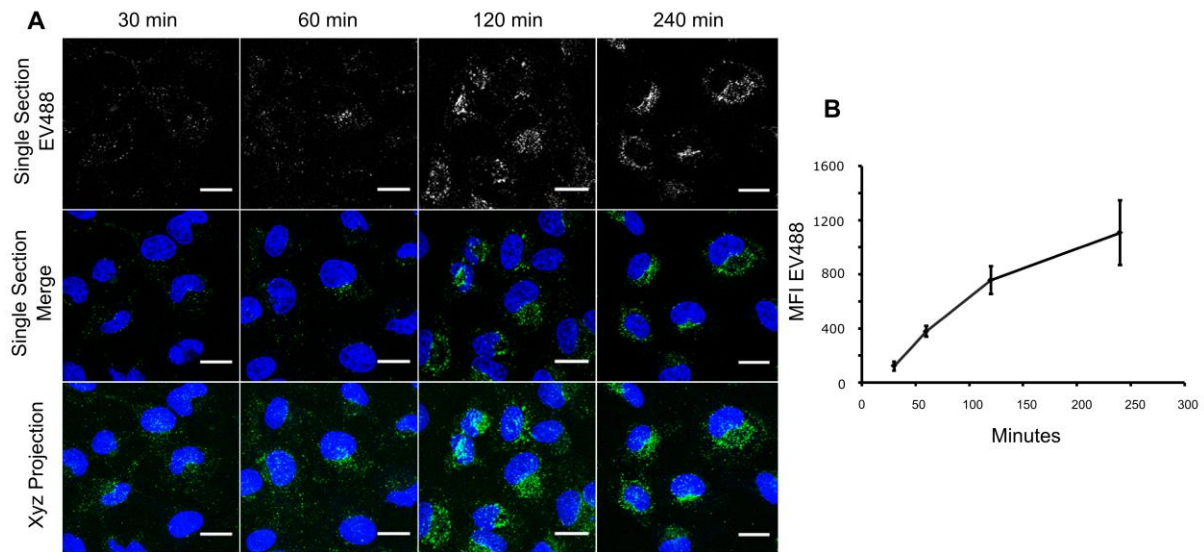


Fig.2. Time dependent EV endocytosis in HeLa cells. (a) Cells were incubated with EV488 (60 $\mu\text{g}/\text{ml}$) for 30, 60, 120 or 240 min and incubated with Hoechst for 5 min before live cell confocal imaging. Scale bars: 20 μm . Images representative of three separate experiments. (b) MFI quantification of the experiments presented. Error bars: Standard error. Representative of three separate experiments.

3.3 Traffic of Alexa488 extracellular vesicles to lysosomes

Cells incubated with EVs for >60 min showed the accumulations of fluorescence in the perinuclear region suggesting a fraction were being trafficked to lysosomes that are also prominent in this region in HeLa cells (Fig. 2)⁴⁵. EV traffic from the plasma membrane was then studied at different time points in cells containing labelled lysosomes via a pulse-chase incubation. Colocalisation between 488-EVs and 647-lysosomes was barely detected at 30 min and then increased over a period of six hours to the point that after 360 min ~60% of detected EVs were contained in labelled lysosomes (Fig. 3). This method measures the location of EVs in early and late endocytic compartments including lysosomes. We then performed experiments by which dextran was similarly used to label lysosomes but following a two hour pulse of EV endocytosis the cells were washed and the material already associated with the cells was chased for a further 4 hour revealing that over 60% of EV associated labelling had reached and remained at the lysosomes by the end of this chase period (Fig. S2).

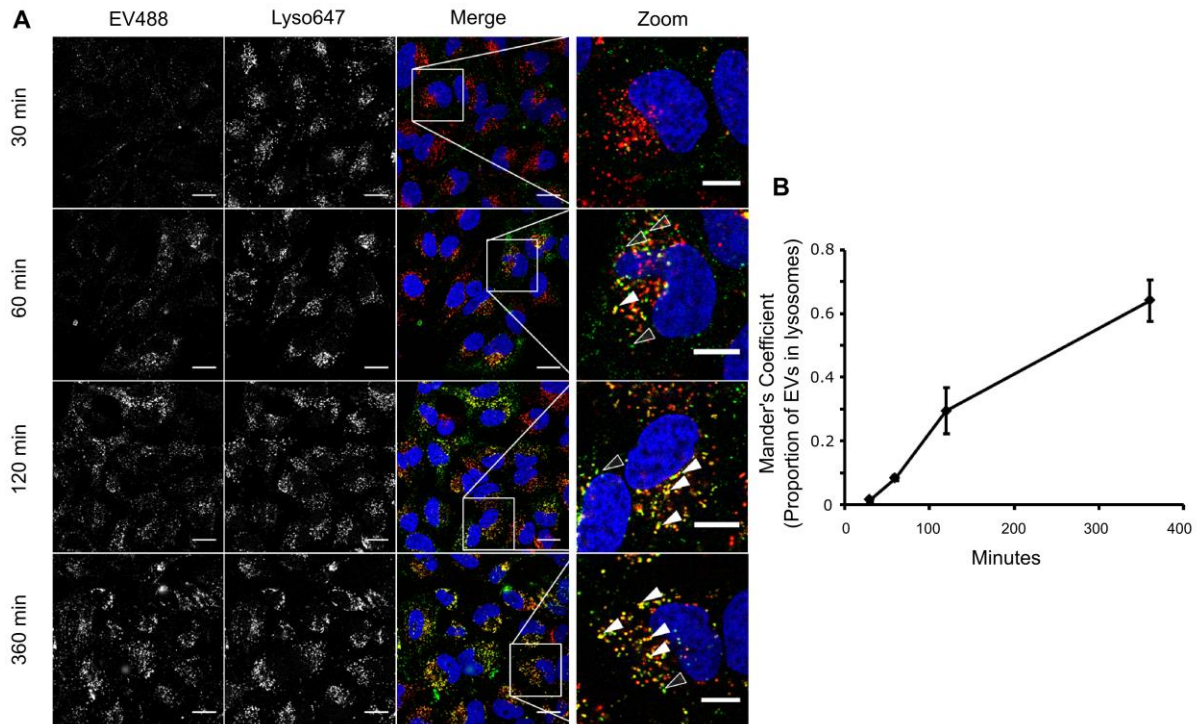


Fig.3. Co-localisation of 488-labelled EVs with dextran-loaded lysosomes in HeLa cells. (a) Cells were incubated with Dx647 (100 $\mu\text{g}/\text{ml}$) for 2 h, washed with PBS and incubated for a further 18 h in culture media. Cells were then incubated with EV488 (60 $\mu\text{g}/\text{ml}$) for either 30, 60, 120 or 360 min before treatment with Hoechst for 5 min and live cell confocal imaging. Solid arrowheads indicate colocalisation between EVs and lysosomes and transparent arrowheads indicate EVs not colocalised with lysosomes. Scale bars: 20 μm and 10 μm in zoomed images. Images representative of three separate experiments. (b) Mander's correlation coefficient analysis of the proportion of green fluorescence (EVs) associated with far-red fluorescence (lysosomes) based on the experiments performed to generate Fig 3A. Error bars: Standard error. Representative of three separate experiments.

3.4 Endocytic Uptake of Extracellular vesicles in Clathrin-mediated endocytosis (CME)

Compromised Cells

CME has been extensively characterised in *in vitro* models including HeLa cells^{10, 11}, and this process can be attenuated using a range of methods³⁴. These include siRNA depletion of a key member of the of the CME adaptor complex AP2, known as AP2 μ 2 or AP50. This subunit is essential for the anchorage of cargo at the plasma membrane and subsequent recruitment of clathrin and further regulatory proteins to allow the process of internalisation to proceed⁴⁶. We and others have shown that siRNA depletion of AP2 μ 2 prevents the uptake of transferrin via the transferrin receptor^{45, 47}. Following a 48 hour transfection with siRNA the AP2 μ 2 protein (50 kDa) was effectively depleted versus a

control siRNA (Fig. 4A). A second siAP2 μ 2 insensitive lower molecular weight band was identified with this antibody that was insensitive to siRNA AP2 μ 2, this has previously been shown but not explained⁴⁸. In these siAP2 μ 2 treated cells incubated with Tf488 for 15 min, the probe was mainly sequestered at the plasma membrane compared to internalised punctate structures in control cells (Fig. 4B). si-control and AP2 μ 2 depleted cells were also incubated with EV488 for 60 min prior to analysing cell fluorescence. Fig. 4C shows no noticeable difference in either the cell fluorescence or the distribution of vesicular labelling between these two conditions. This was further confirmed by quantification of the mean fluorescence intensity (MFI) from three separate analyses including cells that were not transfected (Fig. 4D).

Extracellular vesicle uptake was also evaluated in cells treated with a widely used dynamin II inhibitor, Dynasore, previously used in numerous studies to evaluate the uptake of different entities via dynamin-dependant endocytic processes, such as CME and caveolae⁴⁹. Cells were pre-incubated with Dynasore for 30 min prior to addition of Tf488 for 15 min or EV488 for 60 min. Both the confocal microscopy images and MFI data highlight the strong inhibition of Tf488 uptake by this drug (Fig. 4E-F). Unlike the AP2 μ 2 phenotype showing strong Tf488 labelling on the plasma membrane, Dynasore treated cells were almost devoid of any labelling; the reason for this is currently unknown but suggests that Tf is unable to access its receptor in Dynasore treated cells. There was a much smaller but significant decrease in EV uptake in Dynasore treated cells (Fig. 4E-F). This observation shows that a significant proportion of EVs are entering via a dynamin II-dependant mechanism that based on data in Fig. 4C is not CME. Interestingly cells transfected with a dominant negative dynamin II mutant were also shown to have reduced exosome uptake in RAW 264.7 macrophages²³. Our observation of EV uptake, by a Dynasore but not an AP2 μ 2 dependent process, could be due to the fact dynamin II has been implicated in the regulation of other endocytic pathways such as fluid-phase uptake and caveolae^{50, 51}. Furthermore, it has recently been demonstrated that Dynasore elicits additional dynamin independent effects on the cholesterol organisation of plasma membrane lipid rafts⁵². Alteration of the plasma membrane in this way could affect the wider endocytic network, thereby affecting the designated uptake route of these structures. These studies led to further investigations targeting other endocytic proteins and pathways.

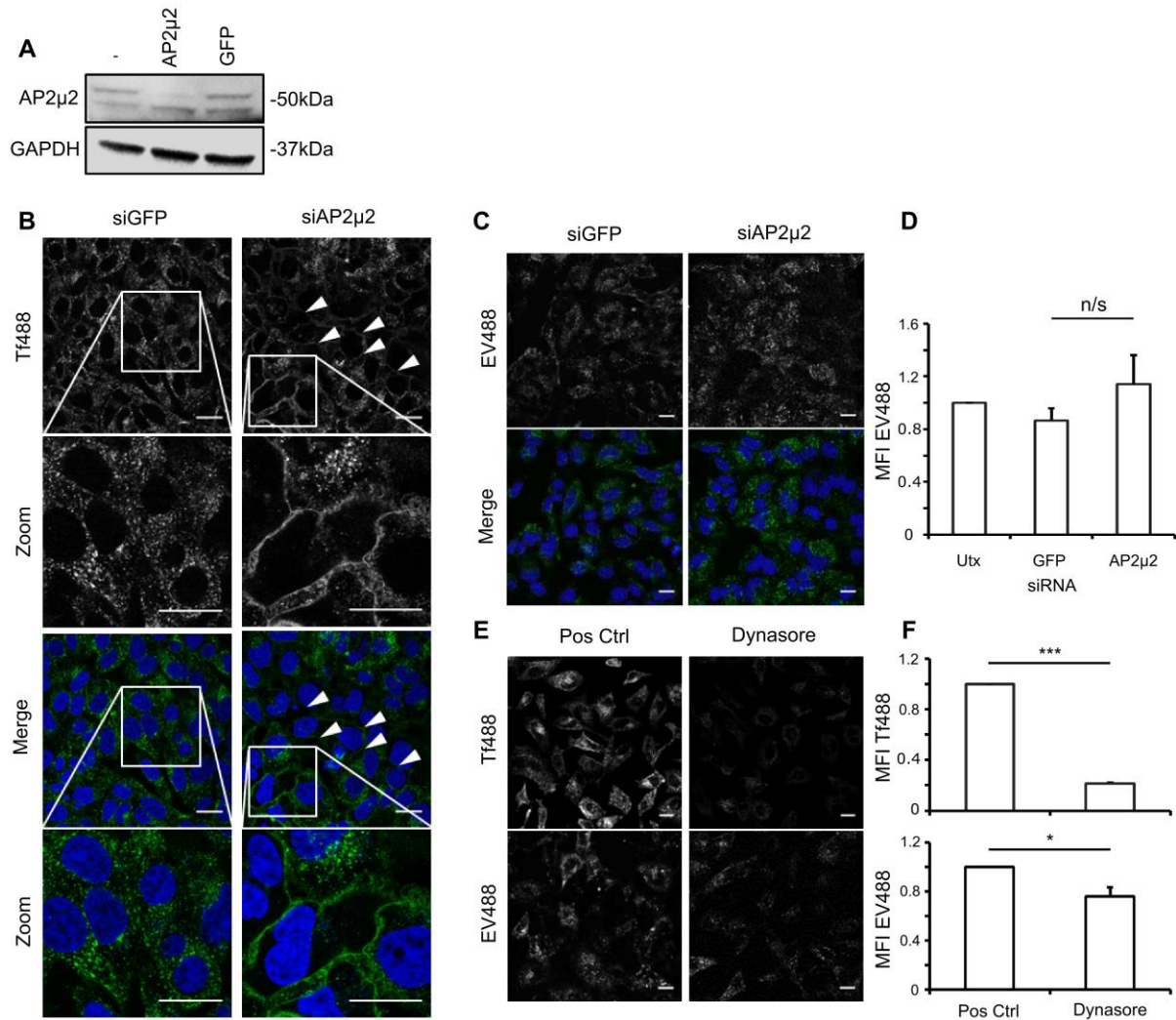


Fig.4. Internalisation of EVs in CME compromised HeLa cells. (a) Western blot analysis of AP2 μ 2 protein levels 48 hr following siRNA transfection in comparison with loading GAPDH loading control. (b) Cells were depleted of either AP2 μ 2 via siRNA transfection for 48 h before incubation with either (b) Tf488 (5 μ g/ml) for 15 min or (c) EV488 (50 μ g/ml) for 60 min. White arrowheads indicate surface bound Tf488. (e) Cells were pre-incubated with Dynasore (80 μ M) for 30 min before incubation with either Tf488 (5 μ g/ml) for 15 min or EV488 (50 μ g/ml) for 60 min. All were incubated with Hoechst for 5 min before live cell imaging. Scale bars: 20 μ m. Images representative of three separate experiments. (d), (f) MFI quantification of the experiments presented in (c), (e), respectively. Utx: Untransfected. Error bars represent Standard error. * p <0.05, *** p <0.001, n/s: No significance. Representative of three separate experiments.

3.5 Extracellular vesicle uptake in Caveolin-1 and Flotillin-1 depleted cells

Using the same siRNA-based approach, both Caveolin-1 and Flotillin-1 proteins were successfully depleted but the loss of these proteins, and the endocytosis that they organise, did not significantly affect cellular uptake of the labelled EVs (Fig. 5). Although not

performed for the studies presented here, we and others have however shown that endocytosis of lactosyl-ceramide and an anti-CD59 antibody have previously been shown to be reduced, respectively, in Caveolin-1 and Flotillin-1 depleted cells^{34, 53}. It should be noted that depletion of either of these proteins could have significant cellular effects beyond that of reducing endocytic processes as both have been implicated as important modulators of cell signalling and organisation of lipid rafts⁵⁴. Of interest is that the distribution of EV labelling was more peripheral in siRNA Flotillin-1 cells compared with controls suggesting alterations in downstream endocytic traffic. Overall these observations strongly suggest that endocytic processes involving Caveolin-1 and Flotillin-1 are not the primary mode of EV entry.

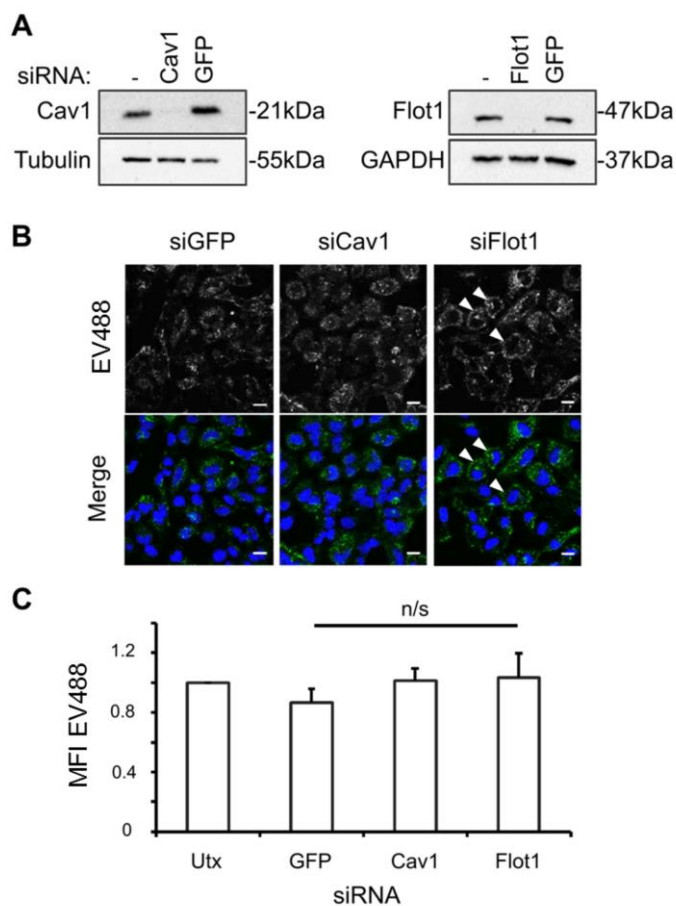


Fig.5. Internalisation of EVs in HeLa cells depleted of Cav-1 and Flot-1. (a) Western blot analysis of Cav-1 and Flot-1 protein levels in HeLa cells 48 h following siRNA transfection in comparison with loading proteins Tubulin or GAPDH. (b) Cells were depleted of either Cav-1 or Flot-1 via siRNA transfection for 48 h before 60 min incubation with EV488 (50 µg/ml). Cells were incubated with Hoechst for 5 min before live cell imaging. Scale bar: 20 µm. Images representative of three separate experiments. Arrowheads in B represent peripheral EVs (c) MFI quantification of the experiments presented in (b). Utx: Untransfected. Error bars represent Standard error. n/s: No significance. Representative of three separate experiments.

3.6 *Extracellular vesicle uptake in cells depleted of proteins regulating actin dynamics, fluid-phase endocytosis and macropinocytosis*

Fluid-phase endocytosis could be viewed as a process of constitutive plasma membrane turnover performed important for functions such as nutrient gathering and sampling of the extracellular environment. Macropinocytosis has been described as a mechanism that is activated upon growth factor stimulation and could be conceived as an activated form of fluid-phase endocytosis^{14, 15, 55, 56}. Both lack a specific master regulatory protein that could be targeted for siRNA depletion without affecting other processes. Macropinocytosis is highly reliant upon the organisation of actin, thus actin regulating proteins are candidate siRNA targets for inhibition of this process. Actin may also have involvement in constitutive fluid phase uptake⁵⁷. The p21-activated kinases (PAKs) regulate numerous modifications of the cytoskeleton, particularly through their interactions with the Rho GTPases, Cdc42 and Rac1^{58, 59}. PAK-1 has been identified as an important regulatory factor in the events associated with macropinocytosis^{18, 19}. Cells were successfully transfected with siRNA sequences targeting PAK-1 and Cdc42 (Fig. 6A) to investigate the roles of these proteins on initially the uptake of dextran that represents in the absence of growth factor activation, a constitutive fluid phase probe^{60, 61}. Our previous studies indicated that PAK-1 was involved in the cellular uptake of cationic cell penetrating peptides that may be inducing a form of macropinocytosis for cell entry^{34, 62}. Despite some visual evidence of a reduction of dextran uptake in PAK-1 depleted cells (Fig. 6B), quantitative analysis showed that this was not significant and no effects were also noted for Cdc42 depletion (Fig. 6C). Following a 60 min endocytic pulse in the cells depleted of either PAK-1 or Cdc42 (Fig. 6D), a small but insignificant decrease (Fig. 6E) in EV uptake was observed. Localisation of punctate EV structures in Cdc42 depleted cells was noticeably different from control cells, being much more apparent at the cell periphery suggesting an inability of these structures to be trafficked beyond the plasma membrane region (Fig. 6D). These observations are further represented in the additional fields of view presented in Fig. S3. As noted for Flotillin-1 and Caveolin-1 the effects of depleting these proteins scope wider than endocytosis but the data suggest that traffic of EVs beyond the plasma membrane is regulated by Cdc42 and most probably actin. Actin regulating agents such as Cytochalasin D are routinely used to monitor

the involvement of actin on endocytosis but they also cause gross morphological effects on cells (data not shown) making data interpretation very difficult.

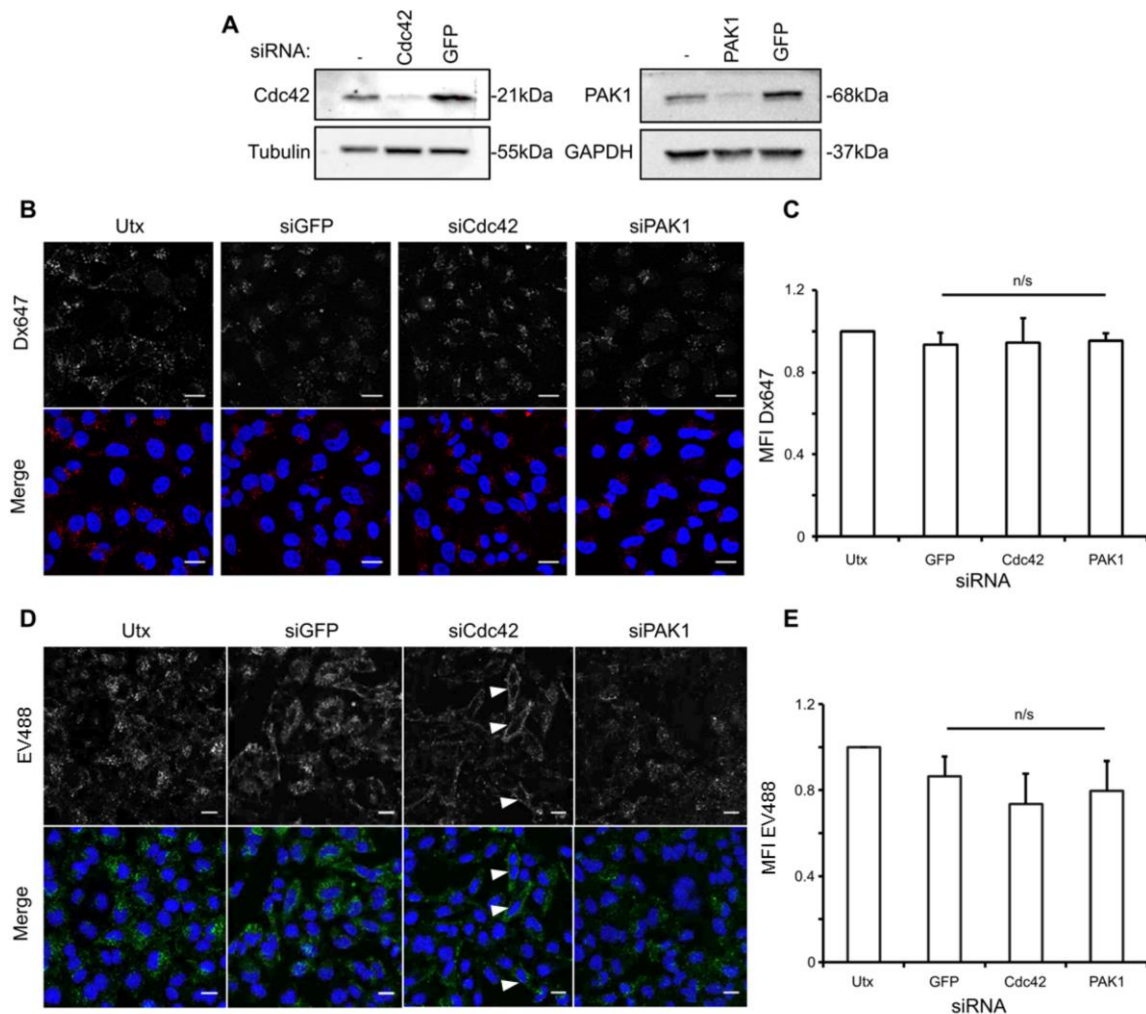


Fig.6. Internalisation of EVs in HeLa cells depleted of fluid-phase/macropinocytosis related proteins. (a) Western blot analysis of Cdc42 and PAK-1 protein levels in cells 48 h following siRNA transfection in comparison with loading proteins Tubulin or GAPDH. (b) Cells were depleted of either Cdc42 or PAK-1 via siRNA transfection for 48 h before 60 min incubation with either (b) Dx488 (100 μ g/ml) or (d) EV488 (50 μ g/ml). Cells were incubated with Hoechst for 5 min before live cell imaging. Arrowheads in D represent peripheral EVs. Utx: Untransfected. Scale bar: 20 μ m. Images representative of three separate experiments, respectively. (c), (e) MFI quantification of the experiments presented in (b), (d), respectively. Error bars represent Standard error. n/s: No significance. Representative of three separate experiments, respectively.

3.7 Extracellular vesicle uptake in cells treated with fluid-phase/macropinocytosis inhibitors

Endocytosis inhibitors can be used in conjunction with siRNA transfection studies to provide a more comprehensive analysis of the endocytic uptake of different probes⁵³. Following our observations in siPAK-1 and siCdc42 cells, inhibitors targeting fluid-phase endocytosis and macropinocytosis were utilised to further explore the involvement of these pathways in EV uptake.

5-(N-Ethyl-N-isopropyl) amiloride (EIPA) is a commonly utilised Na⁺/H⁺ exchange inhibitor, and most probably prevents macropinocytosis by lowering the submembranous pH of the macropinocytic cup⁶³. A small but insignificant (p=0.61) decrease in dextran uptake was observed in EIPA treated cells (Fig. 7A-B), suggesting that it has little effect on fluid-phase endocytosis. Transferrin internalisation in these cells in comparison with control treated cells was significantly reduced, indicating that EIPA affects CME to a certain degree (Fig. S4). Notably, differences in the localisation of transferrin loaded vesicles was apparent, agreeing with our previous studies showing effects on the subcellular localisation of early and late endosomes/lysosomes in cells treated with this drug⁶⁴. Previous studies in PC12 cells incubated with self-derived exosomes have shown by flow cytometry that EIPA significantly reduces uptake of DiD labelled PC12 exosomes²⁶. In our study EIPA cells caused a small but insignificant decrease in EV uptake (Fig. 7C-D). Rottlerin is an inhibitor primarily utilised to target fluid-phase endocytosis rather than macropinocytosis⁶¹. Its effects have previously been connected with inhibition of PKC δ activity⁶⁵, though other Rottlerin targets have been identified^{66, 67}. Rottlerin did not affect the uptake of dextran but was a significant inhibitor of Tf and EV uptake in these cells (44% and 51% respectively) (Fig. 7 and S4). The PAK-1 inhibitor IPA-3⁶⁸, has previously been used to propose macropinocytosis as a mechanism for viral cell entry^{69, 70}. This drug induced a significant decrease in dextran uptake (60%) and EVs (50%, Fig. 7) with Tf488 showing a slight, non-significant decrease. However, Tf488 localisation was more scattered in treated cells (Fig. S4) with a concomitant loss of juxtannuclear polarisation that is indicative of the localisation of Tf recycling compartments in this cell line. Collectively observations with these inhibitors suggest that a major fraction of EVs enter cells by fluid phase endocytosis rather than macropinocytosis.

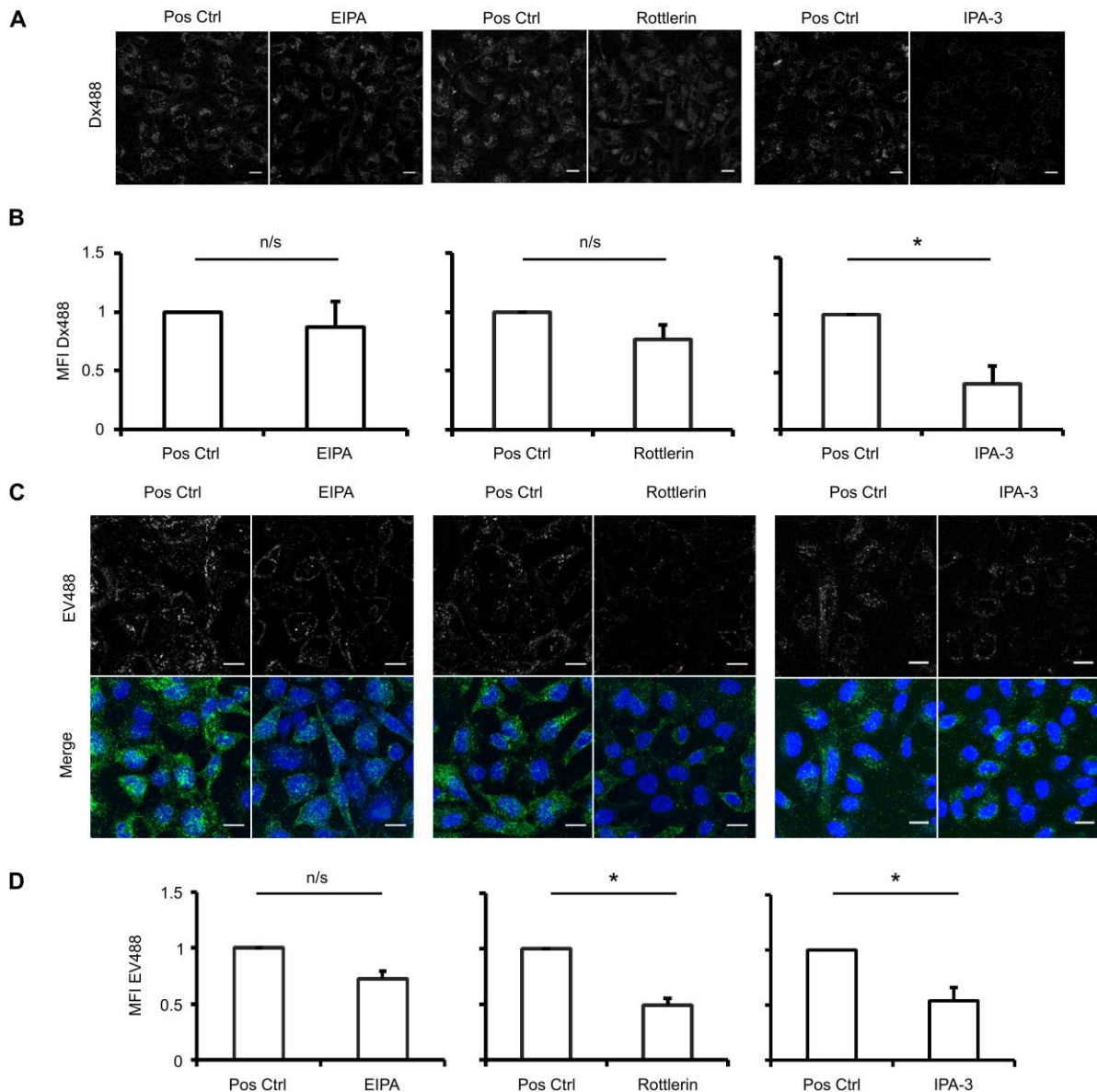


Fig.7. Internalisation of EVs in HeLa cells treated with fluid-phase/macropinocytosis inhibitors. (a,c) Cells were pre-incubated with EIPA (25 μ M), Rottlerin (10 μ M), IPA-3 (50 μ M), or 0.05% DMSO as 'Pos Ctrl' for 30 min before 60 min incubation with either (a) Dx488 (100 μ g/ml) or (c) EV488 (50 μ g/ml). Cells were incubated with Hoechst for 5 min before live cell imaging. Scale bar: 20 μ m. Images representative of three separate experiments. (b), (d) MFI quantification of the experiments presented in (a), (c), respectively. Error bars represent Standard error. * $p < 0.05$. n/s: No significance. Representative of three separate experiments.

4 Conclusions

Here we describe an efficient and novel method to fluorescently label EVs characterised as exosomes for subsequent high content microscopy analysis of their interactions with cells

and endocytic traffic. Unlike other current labelling methods, this technique provides flexibility with regards to choice of fluorophore used and also provides the ability to easily label EVs from different cell types. In the case of prostate cancer DU145 derived EVs the labelling procedure did not affect their capacity to induce complex cellular responses such as fibroblast to myofibroblast differentiation and induction of HGF secretion. It however remains to be determined whether this labelling method influences the other numerous functional effects documented for EVs. It will also be interesting to compare our data with exosomes labelled using the same procedure but with different fluorophores, noting that they have unique characteristics that could affect cell uptake ⁷¹ and differentiation. Interference of endocytic pathways with inhibitors and siRNA depletion of endocytosis mediators together with endocytic trafficking studies strongly suggest our EVs enter cells as components of the extracellular fluid and like dextran are mostly trafficked to lysosomes. Approximately 40% of endocytosed EVs however are not fated for lysosomes, at least within the time-frame that we have explored. The implications of these endocytosis characteristics for the use of EVs as drug delivery vectors remain to be determined but their trafficking profiles may be beneficially exploited if they can be packaged with small molecule drugs for lysosomal release into the cytosol.

Acknowledgements

The research leading to these results has received support from the Innovative Medicines Initiative Joint Undertaking under grant agreement n° [115363], resources of which are composed of financial contribution from the European Union's Seventh Framework Programme (FP7/2007-2013) and EFPIA companies' in kind contribution (HDRD, EJS, PW, ATJ). This work was also supported by Tenovus (ACo, ACI, PW, ATJ) and Prostate Cancer UK (PCUK – award n° CDF13-001, JW).

References

1. G. Raposo, H. W. Nijman, W. Stoorvogel, R. Liejendekker, C. V. Harding, C. J. Melief and H. J. Geuze, *The Journal of experimental medicine*, 1996, **183**, 1161-1172.
2. M. Ostrowski, N. B. Carmo, S. Krumeich, I. Fanget, G. Raposo, A. Savina, C. F. Moita, K. Schauer, A. N. Hume, R. P. Freitas, B. Goud, P. Benaroch, N. Hacohen, M. Fukuda, C. Desnos, M. C. Seabra, F. Darchen, S. Amigorena, L. F. Moita and C. Thery, *Nature cell biology*, 2010, **12**, 19-30; sup pp 11-13.
3. H. Kalra, R. J. Simpson, H. Ji, E. Aikawa, P. Altevogt, P. Askenase, V. C. Bond, F. E. Borrás, X. Breakefield, V. Budnik, E. Buzas, G. Camussi, A. Clayton, E. Cocucci, J. M. Falcon-Perez, S. Gabrielsson, Y. S. Gho, D. Gupta, H. C. Harsha, A. Hendrix, A. F. Hill, J. M. Inal, G. Jenster, E. M. Kramer-Albers, S. K. Lim, A. Llorente, J. Lotvall, A. Marcilla, L. Mincheva-Nilsson, I. Nazarenko, R. Nieuwland, E. N. Nolte-'t Hoen, A. Pandey, T. Patel, M. G. Piper, S. Pluchino, T. S. Prasad, L. Rajendran, G. Raposo, M. Record, G. E. Reid, F. Sanchez-Madrid, R. M. Schiffelers, P. Siljander, A. Stensballe, W. Stoorvogel, D. Taylor, C. Thery, H. Valadi, B. W. van Balkom, J. Vazquez, M. Vidal, M. H. Wauben, M. Yanez-Mo, M. Zoeller and S. Mathivanan, *PLoS biology*, 2012, **10**, e1001450.
4. Z. Andreu and M. Yanez-Mo, *Frontiers in immunology*, 2014, **5**, 442.
5. M. P. Zaborowski, L. Balaj, X. O. Breakefield and C. P. Lai, *Bioscience*, 2015, **65**, 783-797.
6. M. Yanez-Mo, P. R. Siljander, Z. Andreu, A. B. Zavec, F. E. Borrás, E. I. Buzas, K. Buzas, E. Casal, F. Cappello, J. Carvalho, E. Colas, A. Cordeiro-da Silva, S. Fais, J. M. Falcon-Perez, I. M. Ghobrial, B. Giebel, M. Gimona, M. Graner, I. Gursel, M. Gursel, N. H. Heegaard, A. Hendrix, P. Kierulf, K. Kokubun, M. Kosanovic, V. Kralj-Iglic, E. M. Kramer-Albers, S. Laitinen, C. Lasser, T. Lener, E. Ligeti, A. Line, G. Lipps, A. Llorente, J. Lotvall, M. Mancek-Keber, A. Marcilla, M. Mittelbrunn, I. Nazarenko, E. N. Nolte-'t Hoen, T. A. Nyman, L. O'Driscoll, M. Olivan, C. Oliveira, E. Pallinger, H. A. Del Portillo, J. Reventos, M. Rigau, E. Rohde, M. Sammar, F. Sanchez-Madrid, N. Santarem, K. Schallmoser, M. S. Ostenfeld, W. Stoorvogel, R. Stukelj, S. G. Van der Grein, M. H. Vasconcelos, M. H. Wauben and O. De Wever, *Journal of extracellular vesicles*, 2015, **4**, 27066.
7. E. V. Batrakova and M. S. Kim, *Journal of controlled release : official journal of the Controlled Release Society*, 2015, **219**, 396-405.
8. P. Vader, E. A. Mol, G. Pasterkamp and R. M. Schiffelers, *Advanced drug delivery reviews*, 2016, **106**, 148-156.
9. G. J. Doherty and H. T. McMahon, *Annual review of biochemistry*, 2009, **78**, 857-902.
10. H. T. McMahon and E. Boucrot, *Nature reviews. Molecular cell biology*, 2011, **12**, 517-533.
11. M. S. Robinson, *Traffic (Copenhagen, Denmark)*, 2015, **16**, 1210-1238.
12. B. Nichols, *Journal of cell science*, 2003, **116**, 4707-4714.
13. T. Ait-Slimane, R. Galmes, G. Trugnan and M. Maurice, *Molecular biology of the cell*, 2009, **20**, 3792-3800.
14. A. T. Jones, *Journal of cellular and molecular medicine*, 2007, **11**, 670-684.
15. M. C. Kerr and R. D. Teasdale, *Traffic (Copenhagen, Denmark)*, 2009, **10**, 364-371.
16. J. A. Swanson, *Nature reviews. Molecular cell biology*, 2008, **9**, 639-649.
17. J. Mercer, S. Knebel, F. I. Schmidt, J. Crouse, C. Burkard and A. Helenius, *Proceedings of the National Academy of Sciences of the United States of America*, 2010, **107**, 9346-9351.
18. S. Dharmawardhane, A. Schurmann, M. A. Sells, J. Chernoff, S. L. Schmid and G. M. Bokoch, *Molecular biology of the cell*, 2000, **11**, 3341-3352.
19. P. Liberali, E. Kakkonen, G. Turacchio, C. Valente, A. Spaar, G. Perinetti, R. A. Bockmann, D. Corda, A. Colanzi, V. Marjomaki and A. Luini, *The EMBO journal*, 2008, **27**, 970-981.
20. C. Escrevente, S. Keller, P. Altevogt and J. Costa, *BMC cancer*, 2011, **11**, 108.

21. A. Montecalvo, A. T. Larregina, W. J. Shufesky, D. B. Stolz, M. L. Sullivan, J. M. Karlsson, C. J. Baty, G. A. Gibson, G. Erdos, Z. Wang, J. Milosevic, O. A. Tkacheva, S. J. Divito, R. Jordan, J. Lyons-Weiler, S. C. Watkins and A. E. Morelli, *Blood*, 2012, **119**, 756-766.
22. L. A. Mulcahy, R. C. Pink and D. R. Carter, *Journal of extracellular vesicles*, 2014, **3**.
23. D. Feng, W. L. Zhao, Y. Y. Ye, X. C. Bai, R. Q. Liu, L. F. Chang, Q. Zhou and S. F. Sui, *Traffic (Copenhagen, Denmark)*, 2010, **11**, 675-687.
24. G. Sagar, R. P. Sah, N. Javeed, S. K. Dutta, T. C. Smyrk, J. S. Lau, N. Giorgadze, T. Tchkonja, J. L. Kirkland, S. T. Chari and D. Mukhopadhyay, *Gut*, 2016, **65**, 1165-1174.
25. O. P. Wiklander, J. Z. Nordin, A. O'Loughlin, Y. Gustafsson, G. Corso, I. Mager, P. Vader, Y. Lee, H. Sork, Y. Seow, N. Heldring, L. Alvarez-Erviti, C. I. Smith, K. Le Blanc, P. Macchiarini, P. Jungebluth, M. J. Wood and S. E. Andaloussi, *Journal of extracellular vesicles*, 2015, **4**, 26316.
26. T. Tian, Y. L. Zhu, Y. Y. Zhou, G. F. Liang, Y. Y. Wang, F. H. Hu and Z. D. Xiao, *The Journal of biological chemistry*, 2014, **289**, 22258-22267.
27. J. D. Tario, Jr., K. Humphrey, A. D. Bantly, K. A. Muirhead, J. S. Moore and P. K. Wallace, *Journal of visualized experiments : JoVE*, 2012, DOI: 10.3791/4287, e4287.
28. V. V. Temchura, M. Tenbusch, G. Nchinda, G. Nabi, B. Tippler, M. Zelenyuk, O. Wildner, K. Uberla and S. Kuate, *Vaccine*, 2008, **26**, 3662-3672.
29. A. Suetsugu, K. Honma, S. Saji, H. Moriwaki, T. Ochiya and R. M. Hoffman, *Advanced drug delivery reviews*, 2013, **65**, 383-390.
30. I. Nakase, N. B. Kobayashi, T. Takatani-Nakase and T. Yoshida, *Scientific reports*, 2015, **5**, 10300.
31. D. Perez-Hernandez, C. Gutierrez-Vazquez, I. Jorge, S. Lopez-Martin, A. Ursa, F. Sanchez-Madrid, J. Vazquez and M. Yanez-Mo, *The Journal of biological chemistry*, 2013, **288**, 11649-11661.
32. J. Webber, R. Steadman, M. D. Mason, Z. Tabi and A. Clayton, *Cancer research*, 2010, **70**, 9621-9630.
33. J. P. Webber, L. K. Spary, A. J. Sanders, R. Chowdhury, W. G. Jiang, R. Steadman, J. Wymant, A. T. Jones, H. Kynaston, M. D. Mason, Z. Tabi and A. Clayton, *Oncogene*, 2015, **34**, 290-302.
34. M. Al Soraj, L. He, K. Peynshaert, J. Cousaert, D. Vercauteren, K. Braeckmans, S. C. De Smedt and A. T. Jones, *Journal of controlled release : official journal of the Controlled Release Society*, 2012, **161**, 132-141.
35. J. P. Mitchell, J. Court, M. D. Mason, Z. Tabi and A. Clayton, *Journal of immunological methods*, 2008, **335**, 98-105.
36. J. Lotvall, A. F. Hill, F. Hochberg, E. I. Buzas, D. Di Vizio, C. Gardiner, Y. S. Ghossein, I. V. Kurochkin, S. Mathivanan, P. Quesenberry, S. Sahoo, H. Tahara, M. H. Wauben, K. W. Witwer and C. Thery, *Journal of extracellular vesicles*, 2014, **3**, 26913.
37. C. Thery, S. Amigorena, G. Raposo and A. Clayton, *Current protocols in cell biology / editorial board, Juan S. Bonifacino ... [et al.]*, 2006, **Chapter 3**, Unit 3.22.
38. R. Linares, S. Tan, C. Gounou and A. R. Brisson, *Methods in molecular biology (Clifton, N.J.)*, 2017, **1545**, 43-54.
39. Z. A. Martínez and M. Yáñez-Mó, *Frontiers in immunology*, 2014, **5**.
40. J. Webber and A. Clayton, *Journal of extracellular vesicles*, 2013, **2**.
41. A. K. Enjeti, L. Lincz and M. Seldon, *International journal of laboratory hematology*, 2008, **30**, 196-199.
42. S. E. Headland, H. R. Jones, A. S. V. D'Sa, M. Perretti and L. V. Norling, *Scientific reports*, 2014, **4**, 5237.
43. I. Nakase and S. Futaki, *Scientific reports*, 2015, **5**, 10112.
44. K. J. Svensson, H. C. Christianson, A. Wittrup, E. Bourseau-Guilmain, E. Lindqvist, L. M. Svensson, M. Morgelin and M. Belting, *The Journal of biological chemistry*, 2013, **288**, 17713-17724.

45. P. R. Moody, E. J. Sayers, J. P. Magnusson, C. Alexander, P. Borri, P. Watson and A. T. Jones, *Molecular therapy : the journal of the American Society of Gene Therapy*, 2015, **23**, 1888-1898.
46. L. P. Jackson, B. T. Kelly, A. J. McCoy, T. Gaffry, L. C. James, B. M. Collins, S. Honing, P. R. Evans and D. J. Owen, *Cell*, 2010, **141**, 1220-1229.
47. A. Motley, N. A. Bright, M. N. Seaman and M. S. Robinson, *The Journal of cell biology*, 2003, **162**, 909-918.
48. J. E. Alford, J. Gumbs and E. C. Anderson, *PloS one*, 2014, **9**, e91429.
49. E. Macia, M. Ehrlich, R. Massol, E. Boucrot, C. Brunner and T. Kirchhausen, *Developmental cell*, 2006, **10**, 839-850.
50. H. Cao, J. Chen, M. Awoniyi, J. R. Henley and M. A. McNiven, *Journal of cell science*, 2007, **120**, 4167-4177.
51. J. R. Henley, E. W. Krueger, B. J. Oswald and M. A. McNiven, *The Journal of cell biology*, 1998, **141**, 85-99.
52. G. Preta, J. G. Cronin and I. M. Sheldon, *Cell communication and signaling : CCS*, 2015, **13**, 24.
53. D. Vercauteren, M. Piest, L. J. van der Aa, M. Al Soraj, A. T. Jones, J. F. Engbersen, S. C. De Smedt and K. Braeckmans, *Biomaterials*, 2011, **32**, 3072-3084.
54. P. Lajoie and I. R. Nabi, *International review of cell and molecular biology*, 2010, **282**, 135-163.
55. J. A. Swanson and C. Watts, *Trends in cell biology*, 1995, **5**, 424-428.
56. J. P. Lim and P. A. Gleeson, *Immunology and cell biology*, 2011, **89**, 836-843.
57. W. Shurety, N. L. Stewart and J. L. Stow, *Molecular biology of the cell*, 1998, **9**, 957-975.
58. D. C. Edwards, L. C. Sanders, G. M. Bokoch and G. N. Gill, *Nature cell biology*, 1999, **1**, 253-259.
59. C. Vidal, B. Geny, J. Melle, M. Jandrot-Perrus and M. Fontenay-Roupie, *Blood*, 2002, **100**, 4462-4469.
60. J. P. Lim, P. Gosavi, J. D. Mintern, E. M. Ross and P. A. Gleeson, *Journal of cell science*, 2015, DOI: 10.1242/jcs.174359.
61. H. Hufnagel, P. Hakim, A. Lima and F. Hollfelder, *Molecular therapy : the journal of the American Society of Gene Therapy*, 2009, **17**, 1411-1417.
62. I. Nakase, M. Niwa, T. Takeuchi, K. Sonomura, N. Kawabata, Y. Koike, M. Takehashi, S. Tanaka, K. Ueda, J. C. Simpson, A. T. Jones, Y. Sugiura and S. Futaki, *Molecular therapy : the journal of the American Society of Gene Therapy*, 2004, **10**, 1011-1022.
63. M. Koivusalo, C. Welch, H. Hayashi, C. C. Scott, M. Kim, T. Alexander, N. Touret, K. M. Hahn and S. Grinstein, *The Journal of cell biology*, 2010, **188**, 547-563.
64. M. Fretz, J. Jin, R. Conibere, N. A. Penning, S. Al-Taei, G. Storm, S. Futaki, T. Takeuchi, I. Nakase and A. T. Jones, *Journal of controlled release : official journal of the Controlled Release Society*, 2006, **116**, 247-254.
65. M. Gschwendt, H. J. Muller, K. Kielbassa, R. Zang, W. Kittstein, G. Rincke and F. Marks, *Biochemical and biophysical research communications*, 1994, **199**, 93-98.
66. S. P. Soltoff, *Trends in pharmacological sciences*, 2007, **28**, 453-458.
67. S. P. Soltoff, *The Journal of biological chemistry*, 2001, **276**, 37986-37992.
68. S. W. Deacon, A. Beeser, J. A. Fukui, U. E. E. Rennefahrt, C. Myers, J. Chernoff and J. R. Peterson, *Chemistry & biology*, 2008, **15**, 322-331.
69. Z. Wen, B. Zhao, K. Song, X. Hu, W. Chen, D. Kong, J. Ge and Z. Bu, *Viral J*, 2013, **10**, 331.
70. M. A. Krzyzaniak, M. T. Zumstein, J. A. Gerez, P. Picotti and A. Helenius, *PLoS Pathog*, 2013, **9**, e1003309.
71. A. T. Jones and E. J. Sayers, *Journal of controlled release : official journal of the Controlled Release Society*, 2012, **161**, 582-91.

Supplementary Materials

Supplementary Materials and Methods

1. Extracellular vesicle (EV) isolation, purification and characterisation

Extracellular vesicles were purified from 7-day cell conditioned media, pre-cleared of cell debris and microvesicles by differential centrifugation followed by filtration through a 0.22 μm filter (Millipore). EVs were purified based on their density by ultracentrifugation at 100,000 $\times g$ on a 30% sucrose/D₂O cushion as described ¹. Purified EVs were resuspended in around 100 μl PBS, aliquoted, before storage at -80°C. Total protein was quantified by microBCA protein assay (ThermoFisher Scientific, Paisley, UK). The number, and size distribution of nano-particles was assessed by nanoparticle tracking analysis (Nanosight; Malvern Instruments, Worcestershire, UK). As a measure of EV purity, protein and nanoparticle concentrations were used to calculate a ratio of particle to protein. All preparations had a particle to protein ratio of $>2 \times 10^{10}$ particles per μg of protein, as described ². The presence of tetraspanins at the outer EV surface was determined using a plate-immobilisation of purified EVs, and indirect staining with antibodies against CD9 (R&D Systems, Abingdon, UK), CD81 or CD63 (BioRad, Hertfordshire, UK), a secondary anti-Mouse IgG-biotin conjugate (PerkinElmer) and streptavidin-Europium detection. Primary antibodies against relevant isotypes, IgG1 and IgG2b (eBioscience, ThermoFisher Scientific), were used as a control. Time resolved fluorometry was performed on a Pherastar FS instrument (BMGlabtech, Germany) as described ³. Whole cell lysates, prepared using RIPA-buffer (Santa Cruz Biotechnology) were compared to EV lysates, prepared by boiling in SDS-sample buffer containing 20 mM DTT, by western blotting running 10 μg protein per lane. After transfer to PVDF membranes (GE Healthcare), and blocking with 5% non-fat powdered milk with 0.1% Tween-20 in PBS for 1 hr, primary monoclonal antibody at a concentration of 1-4 $\mu\text{g}/\text{ml}$ was added at 4°C overnight. Antibodies for expected EV proteins TSG101, Alix, LAMP1 (Santa Cruz Biotechnology), MHC Class I (eBioscience, ThermoFisher Scientific) were used, and to assess cellular contaminants, blots were also probed for calnexin expression (Santa Cruz). After washes in 0.1% Tween-20/PBS

bands were detected using an anti-mouse IgG-horseradish peroxidase conjugated antibody (Santa Cruz) and chemiluminescence substrate (PicoWest, ThermoFisher Scientific). Images of membranes were collected using the C-DiGit Chemiluminescence Blot Scanner (LI-COR Biotechnology, Cambridge, UK).

2. Extracellular vesicle analysis by Nano particle Tracking Analysis (NanoSight™)

Freshly prepared EVs, or those following fluorescent labelling were diluted in particle free water (Fresenius Kabi, Runcorn, UK) to concentrations up to 2×10^9 particles/ml, which is within the linear range of the NanoSight instrument. Analysis was performed on a NanoSight™ NS300 system configured with a temperature controlled LM14 laser module with a 488 nm laser and a high sensitivity sCMOS camera system and a syringe-pump system (Malvern Instruments, Malvern, UK). Three videos of 30-60 s were taken under controlled fluid flow with a pump speed set to 80, and temperature set to 25°C. Videos were taken in light scatter mode. On some occasions, videos were also taken following application of a long-pass fluorescence filter, so that only particles emitting light at >500 nm were visible. This required corrections for focusing, and an adjustment to the camera settings to maximise chances of visualising, and tracking fluorescent nano-particles. Videos were analysed using the batch analysis tool of NTA 2.3 software (version 2.3 build 2.3.5.0033.7-Beta7), where minimum particle size, track length and blur were set at “automatic”. The area under the histogram for each triplicate measurement was averaged and used as a particle concentration measurement.

3. Cryo-electron microscopy of purified extracellular vesicles

Extracellular vesicle preparations were adsorbed onto glow-discharging holey carbon 200-mesh copper grids (Quantifoil Micro Tools GmbH). Grids were vitrified with the aid of a Vitrobot (Maastricht Instruments BV). Vitrified samples were imaged at liquid nitrogen temperature using a JEM-2200FS/CR transmission cryo-electron microscope (JEOL) equipped with a field emission gun and operated at an acceleration voltage of 200 kV.

4. siRNA transfection

In a 6 well plate (or 35 mm imaging dish) 100 pmols siRNA was diluted in 185 μ l Opti-MEM while in a separate container 2 μ l Oligofectamine was diluted with 13 μ l OptiMEM. The two solutions were gently mixed and incubated at room temperature for 30 min. The cells were washed with Opti-MEM and 800 μ l of Opti-MEM was added before dropwise addition of the siRNA complex mixture. Cells were returned to the incubator for 4 h before addition of 500 μ l Opti-MEM containing 30% FCS and incubated for 44 h.

5. SDS PAGE and Western blotting

5.1. Following siRNA depletion

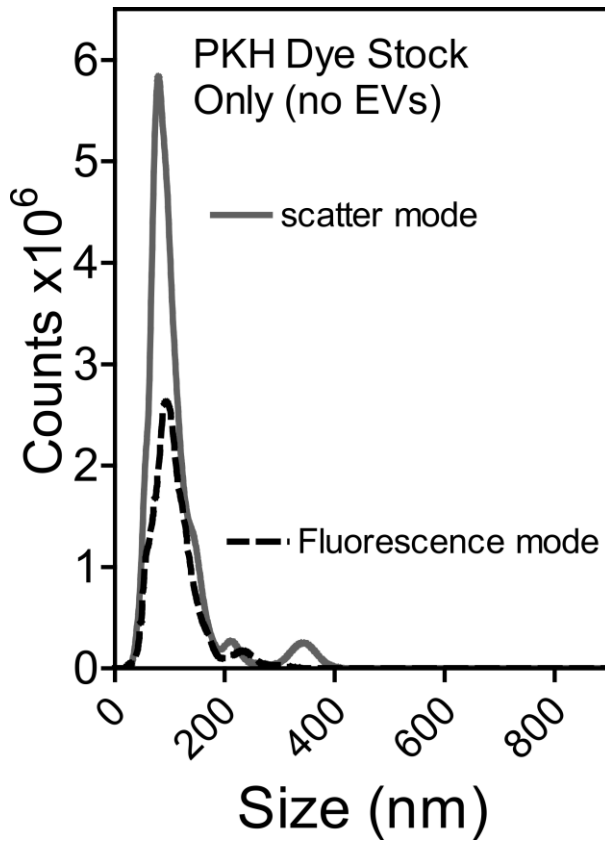
Following 48 h transfection, cells were washed with PBS followed by incubation on ice for 5 min in 100 μ l ice-cold lysis buffer - 150 mM NaCl, 50 mM Tris-base pH 8.0, 1% Triton X-100 containing protease inhibitor cocktail. Cells were scraped from the plastic surface, placed in eppendorf tubes and then centrifuged for 10 min (13000 $\times g$) at 4°C. The protein concentration of each sample was calculated via BCA assay and 18 μ g protein per sample was mixed with 3x SDS PAGE sample buffer, heated to 95°C and loaded on to 8%, 10% or 12% SDS-PAGE gels. Following gel electrophoresis, proteins were transferred to PVDF membranes before blocking (5% w/v dried milk in PBS 0.0025% v/v Tween 20 (PBSTM)) and incubation with primary antibodies recognising AP2 μ 2, Caveolin-1 (Cav-1), Cdc42, Flotillin-1 (Flot-1), p21-activated kinase-1 (PAK-1), or GAPDH in 2% PBSTM. Secondary antibody incubation with goat anti-rabbit HRP conjugate, goat anti-mouse HRP conjugate or HRP conjugated anti- δ -tubulin was then performed and chemiluminescence was detected on a ChemiDoc imager using ImageLab software (Bio-Rad).

6. Optimisation and characterization of extracellular vesicle labelling

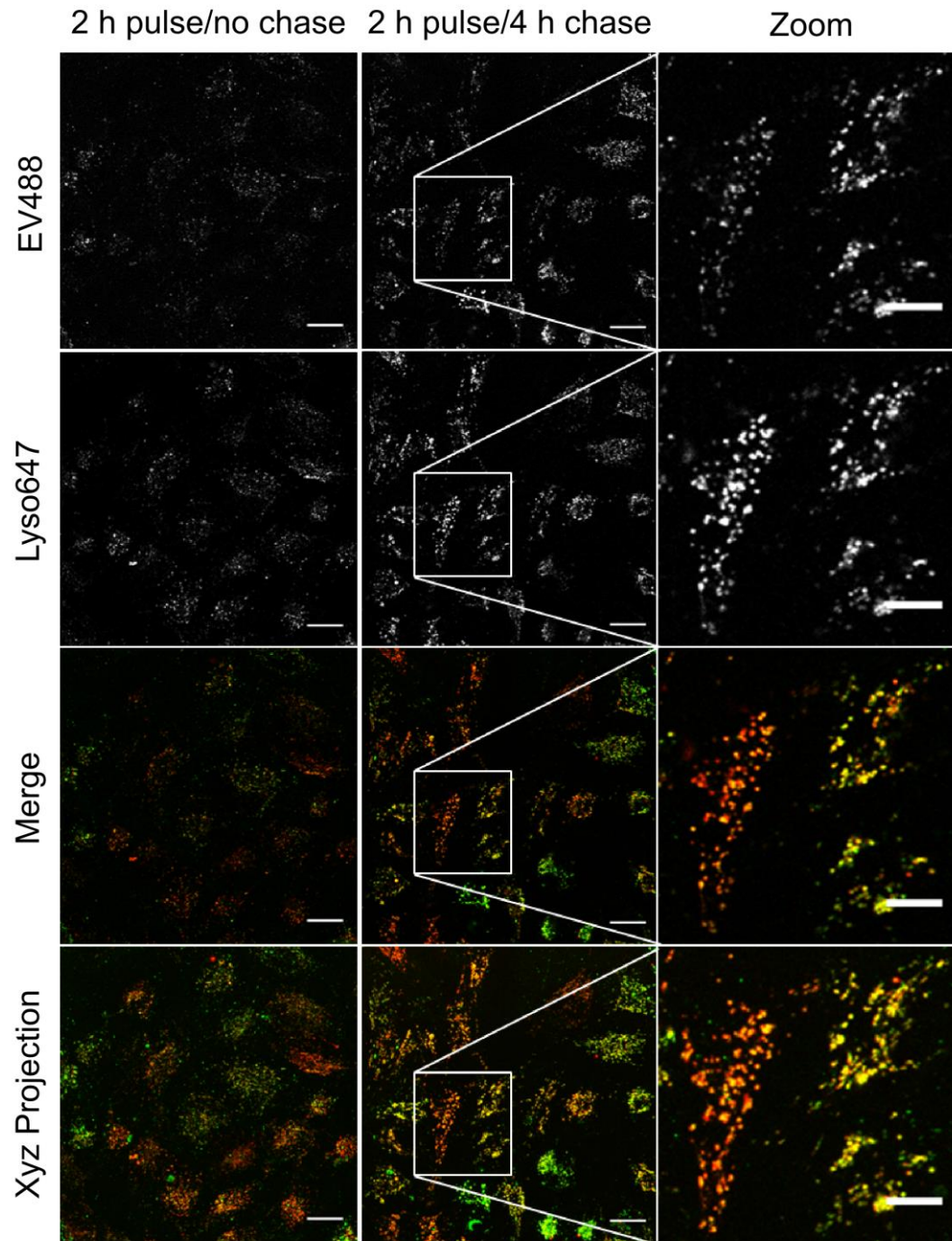
C₅-maleimide-Alexa488 (5-200 μ g/ml) was added to a 30 μ l EV aliquot containing 60 to 100 μ g protein, and made up to a final volume of 50 μ l with PBS. Incubations, with no agitation, for 60 min in the dark at room temperature (R/T), were followed by removal

of unbound dye using exosome spin columns (Invitrogen) according to manufacturer's instructions. Collected labelled EVs were added to black-walled 96-well plates and the average fluorescence of triplicate wells measured on a PHERAstar FS plate reader (BMG Labtech, Ortenberg, Germany). Similarly, at a fixed dose of 200 µg dye, incubations for up to 3 h were performed before assessing intensity of labelling. In parallel, dye in the absence of EVs were included in these experiments, to assess the efficacy of free-dye capture by the exosome spin columns. For some experiments, the free sulph-hydryl bonds at the EV surface were capped by pre incubations with N-acetyl-L-cysteine (up to 1 mM) for 30 min prior to dye labelling (200 µg/ml, 1 h) and fluorescence assessment; revealing approximately 80% inhibition of labelling at maximal N-acetyl-L-cysteine dose.

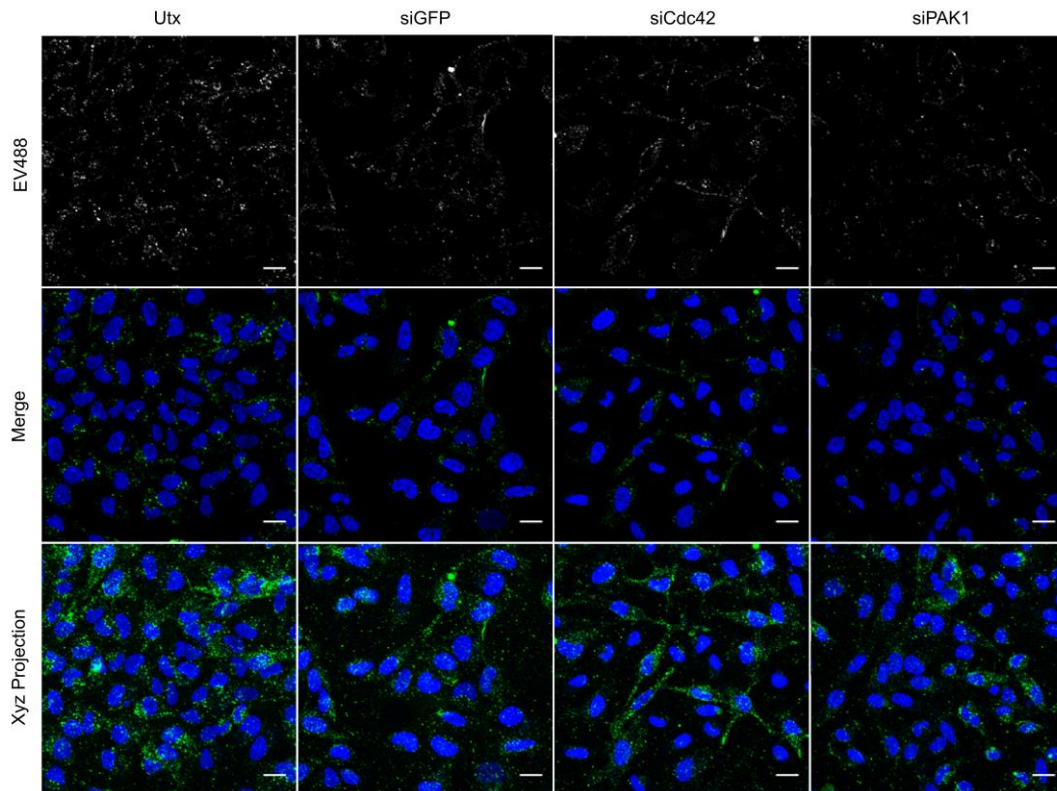
Supplementary Figures



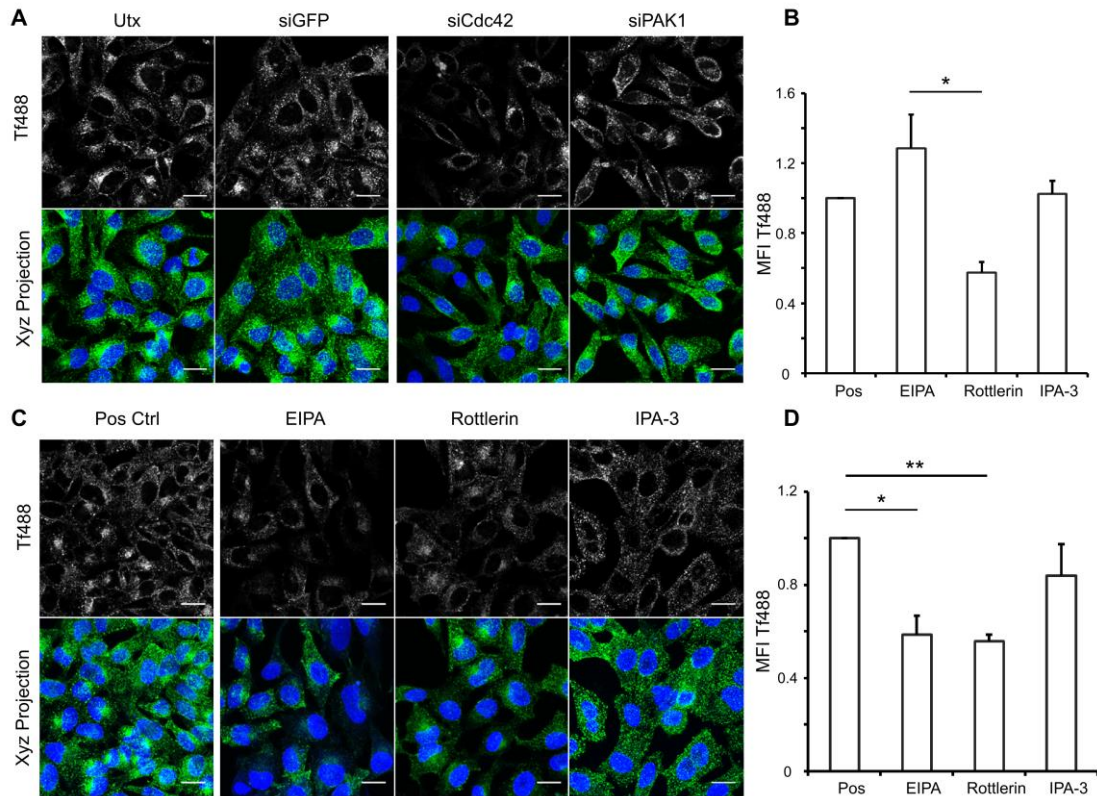
Supplementary Figure. 1. PKH26 dye was diluted 1 in 1000 in the provided dilution buffer, and analysed by NTA. The analysis was performed in light scatter mode (grey), and then following application of fluorescence filter where only fluorescing particles are visible (black, dashed line). We conclude that small particulate material spanning the size range of EVs is present in the stock solution, and a proportion (52%) of these are fluorescent.



Supplementary Figure. 2. Colocalisation of 488-labelled extracellular vesicles with dextran-loaded lysosomes in HeLa cells. Cells were incubated with Dx647 (100 $\mu\text{g}/\text{ml}$) for 2 h, washed with PBS and incubated for a further 18 h in culture media. Cells were then incubated with EV488 (60 $\mu\text{g}/\text{ml}$) for 2h with no chase or for 2 h followed by washing and a 4 hr chase. Scale bars: 20 μm and 10 μm on zoomed images. Images representative of three separate experiments.



Supplementary Figure. 3. Additional fields of view showing internalisation of extracellular vesicles in HeLa cells depleted of fluid-phase/macropinocytosis related proteins. Cells were depleted of either Cdc42 or PAK-1 via siRNA transfection for 48 h before 60 min incubation with EV488 (50 $\mu\text{g}/\text{ml}$). Cells were incubated with Hoechst for 5 min before live cell imaging. Utx: Untransfected. Scale bar: 20 μm . Images representative of three separate experiments.



Supplementary Figure. 4. Transferrin internalisation in HeLa cell models of fluid-phase/macropinocytosis inhibition. (a) Cells were depleted of either Cdc42 or PAK1 via siRNA transfection for 48 h, or (c) pre-incubated with either EIPA (25 μ M), Rottlerin (10 μ M), IPA-3 (50 μ M), or 0.05% DMSO as 'Pos Ctrl' for 30 min before 15 min incubation with Tf488 (5 μ g/ml). Cells were incubated with Hoechst for 5 min before live cell imaging. Scale bar: 20 μ m. Images representative of three separate experiments. (b) and (d) MFI quantification of the experiments presented in (a) and (c), respectively. Error bars represent Standard error. * p <0.05, ** p <0.01. Representative of three separate experiments.

Supplementary Video.1. Time lapse images of EV488 uptake in HeLa cells. EV488 (60 μ g/ml) were added for a period of either 120 min before confocal time lapse imaging. Hoechst and cell mask deep red were added for the final 5 min before imaging. Imaging was continuously performed for a period of 2 min.

Supplementary References

1. C. Thery, S. Amigorena, G. Raposo and A. Clayton, *Current protocols in cell biology / editorial board, Juan S. Bonifacino ... [et al.]*, 2006, **Chapter 3**, Unit 3.22.
2. J. Webber and A. Clayton, *Journal of extracellular vesicles*, 2013, **2**.
3. J. Webber, T. C. Stone, E. Katilius, B. C. Smith, B. Gordon, M. D. Mason, Z. Tabi, I. A. Brewis and A. Clayton, *Molecular & cellular proteomics : MCP*, 2014, **13**, 1050-1064.